

Nearest-Neighbours Neural Network architecture for efficient sampling of statistical physics models

Luca Maria Del Bono,^{1,2} Federico Ricci-Tersenghi,^{1,2,3} and Francesco Zamponi¹

¹*Dipartimento di Fisica, Sapienza Università di Roma, Piazzale Aldo Moro 5, Rome 00185, Italy*

²*CNR-Nanotec, Rome unit, Piazzale Aldo Moro 5, Rome 00185, Italy*

³*INFN, sezione di Roma1, Piazzale Aldo Moro 5, Rome 00185, Italy*

The task of sampling efficiently the Gibbs-Boltzmann distribution of disordered systems is important both for the theoretical understanding of these models and for the solution of practical optimization problems. Unfortunately, this task is known to be hard, especially for spin glasses at low temperatures. Recently, many attempts have been made to tackle the problem by mixing classical Monte Carlo schemes with newly devised Neural Networks that learn to propose smart moves. In this article we introduce the Nearest-Neighbours Neural Network (4N) architecture, a physically-interpretable deep architecture whose number of parameters scales linearly with the size of the system and that can be applied to a large variety of topologies. We show that the 4N architecture can accurately learn the Gibbs-Boltzmann distribution for the two-dimensional Edwards-Anderson model, and specifically for some of its most difficult instances. In particular, it captures properties such as the energy, the correlation function and the overlap probability distribution. Finally, we show that the 4N performance increases with the number of layers, in a way that clearly connects to the correlation length of the system, thus providing a simple and interpretable criterion to choose the optimal depth.

INTRODUCTION

A central problem in many fields of science, from statistical physics to computer science and artificial intelligence, is that of sampling from a complex probability distribution over a large number of variables. More specifically, a very common such probability is a Gibbs-Boltzmann distribution. Given a set of $N \gg 1$ random variables $\boldsymbol{\sigma} = \{\sigma_1, \dots, \sigma_N\}$, such a distribution is written in the form

$$P_{\text{GB}}(\boldsymbol{\sigma}) = \frac{e^{-\beta \mathcal{H}(\boldsymbol{\sigma})}}{\mathcal{Z}(\beta)}. \quad (1)$$

In statistical physics language, the normalization constant $\mathcal{Z}(\beta)$ is called partition function, $\mathcal{H}(\boldsymbol{\sigma})$ is called the Hamiltonian function and $\beta = 1/T$ is the inverse temperature, corresponding to a global rescaling of $\mathcal{H}(\boldsymbol{\sigma})$.

While Eq. (1) is simply a trivial definition, i.e. $\mathcal{H}(\boldsymbol{\sigma}) = -\frac{1}{\beta} \log P_{\text{GB}}(\boldsymbol{\sigma}) + \text{const}$, the central idea of Gibbs-Boltzmann distributions is that $\mathcal{H}(\boldsymbol{\sigma})$ is expanded as a sum of ‘local’ interactions. For instance, in the special case of binary (Ising) variables, $\sigma_i \in \{-1, +1\}$, one can always write

$$\mathcal{H} = - \sum_i H_i \sigma_i - \sum_{i < j} J_{ij} \sigma_i \sigma_j - \sum_{i < j < k} J_{ijk} \sigma_i \sigma_j \sigma_k + \dots \quad (2)$$

In many applications, like in physics (i.e. spin glasses), inference (i.e. maximum entropy models) and artificial intelligence (i.e. Boltzmann machines), the expansion in Eq. (2) is truncated to the pairwise terms, thus neglecting higher-order interactions. This leads to a Hamiltonian

$$\mathcal{H} = - \sum_i H_i \sigma_i - \sum_{i < j} J_{ij} \sigma_i \sigma_j \quad (3)$$

parametrized by ‘local fields’ H_i and ‘pairwise couplings’ J_{ij} . In physics applications such as spin glasses, these are often chosen to be i.i.d. random variables, e.g. $H_i \sim \mathcal{N}(0, H^2)$ and $J_{ij} \sim \mathcal{N}(0, J^2/N)$. In Boltzmann Machines, instead, the fields and couplings are learned by maximizing the likelihood of a given training set.

In many cases, dealing with Eq. (1) analytically, e.g. computing expectation values of quantities of interest, is impossible, and one resorts to numerical computations. A universal strategy is to use *local* Markov Chain Monte Carlo (MCMC) methods, which have the advantage of being applicable to a wide range of different systems. In these methods, one proposes a local move, typically flipping a single spin, $\sigma_i \rightarrow -\sigma_i$, and accepts or rejects the move in such a way to guarantee that after many iterations, the configuration $\boldsymbol{\sigma}$ is distributed according to Eq. (1). Unfortunately, these methods are difficult (if not altogether impossible) to apply in many hard-to-sample problems and, in practice, they may end up taking a huge amount of time. For instance, finding the ground state of the Sherrington-Kirkpatrick model (a particular case of sampling at $T \rightarrow 0$) is known to be a NP-hard problem; sampling a class of optimization problems is known to take a time scaling exponentially with N . The training of Boltzmann Machines is also known to suffer from this kind of problems.

These inconveniences can be avoided by using system-specific *global* algorithms that leverage properties of the system under examination in order to gain a significant speedup. Instead of flipping one spin at a time, these methods are able to construct smart moves, which update simultaneously a large number of spins. An example is the Wolff algorithm [1] for the Ising model. Another class of algorithms uses unphysical moves or extended variable spaces, such as the Swap Monte Carlo for glass-forming models of particles [2]. The downside of these algorithms

is that they cannot generally be transferred from one system to another, meaning that one has to develop new techniques specifically for each system of interest. Yet another class is Parallel Tempering (PT) [3], or one of its modifications [4], which considers a group of systems at different temperatures and alternates between simple MCMC moves and moves that swap the systems at two different temperatures. While PT is a universal strategy, its drawback is that, in order to produce low-temperature configurations, one has to simulate the system at a ladder of higher temperatures, which can be computationally expensive and redundant.

The rise of machine learning technology has sparked a new line of research aimed at using Neural Networks to enhance Monte Carlo algorithms, in the wake of similar approaches in many-body quantum physics [5], molecular dynamics [6] and the study of glasses [7–9]. The key idea is to use the network to propose new states with a probability P_{NN} that (i) can be efficiently sampled and (ii) is close to the Gibbs-Boltzmann distribution, e.g., with respect to the Kullback-Leibler (KL) divergence D_{KL} :

$$D_{\text{KL}}(P_{\text{GB}} \parallel P_{\text{NN}}) = \sum_{\boldsymbol{\sigma}} P_{\text{GB}}(\boldsymbol{\sigma}) \log \frac{P_{\text{GB}}(\boldsymbol{\sigma})}{P_{\text{NN}}(\boldsymbol{\sigma})}. \quad (4)$$

The proposed configurations can be used in a Metropolis scheme, accepting them with probability:

$$\begin{aligned} \text{Acc}[\boldsymbol{\sigma} \rightarrow \boldsymbol{\sigma}'] &= \min \left[1, \frac{P_{\text{GB}}(\boldsymbol{\sigma}') \times P_{\text{NN}}(\boldsymbol{\sigma})}{P_{\text{GB}}(\boldsymbol{\sigma}) \times P_{\text{NN}}(\boldsymbol{\sigma}')} \right] \\ &= \min \left[1, \frac{e^{-\beta\mathcal{H}(\boldsymbol{\sigma}')} \times P_{\text{NN}}(\boldsymbol{\sigma})}{e^{-\beta\mathcal{H}(\boldsymbol{\sigma})} \times P_{\text{NN}}(\boldsymbol{\sigma}')} \right]. \end{aligned} \quad (5)$$

Because \mathcal{H} can be computed in polynomial time and P_{NN} can be sampled efficiently by hypothesis, this approach ensures an efficient sampling of the Gibbs-Boltzmann probability, as long as (i) P_{NN} covers well the support of P_{GB} (i.e., the so-called mode collapse is avoided) and (ii) the acceptance probability in Eq. (5) is significantly different from zero for most of the generated configurations.

The main problem is how to train the Neural Network to minimize Eq. (4); in fact, the computation of D_{KL} requires sampling from P_{GB} . A possible solution is to use $D_{\text{KL}}(P_{\text{NN}} \parallel P_{\text{GB}})$ instead [10], but this has been shown to be prone to mode collapse. Another proposed solution is to set up an iterative procedure, called ‘Sequential Tempering’ (ST), in which one first learns P_{NN} at high temperature where sampling from P_{GB} is possible, then gradually decreases the temperature, updating P_{NN} slowly [11]. It is still unclear whether this kind of strategies actually perform well on hard problems and challenge already-existing algorithms, with both positive [12–14] and negative results [15–18]. First steps in a theoretical understanding of the performances of such algorithms are just being made [19]. A variety of new methods and techniques have thus been proposed to tackle the problem, such as autoregressive models [10, 11], normalizing flows

[20–23], and diffusion models [24]. The main drawbacks of these architectures is that the number of parameters scales poorly with the system size, typically as N^α with $\alpha > 1$, while local Monte Carlo requires a number of operations scaling linearly in N . Furthermore, these architectures – with the notable exception of TwoBo [25] that directly inspired our work – are not informed about the physical properties of the model, and in particular about the structure of its correlations.

In this paper, we introduce the Nearest Neighbours Neural Network, or 4N for short, a Graph Neural Network-inspired architecture that implements an autoregressive scheme to learn the Gibbs-Boltzmann distribution. This architecture has a number of parameters linear in the system size and can sample new configurations in $\mathcal{O}(N)$ time, thus achieving the best possible scaling one could hope for such architectures. Moreover, 4N has a straightforward physical interpretation. In particular, the choice of the number of layers can be directly linked to the correlation length of the model under study. Finally, the architecture can easily be applied to essentially any statistical system, such as lattices in higher dimensions or random graphs, and it is thus more general than other architectures. As a proof of concept, we evaluate the 4N architecture on the two-dimensional Edwards-Anderson spin glass model. We demonstrate that the model succeeds in accurately learning the Gibbs-Boltzmann distribution, especially for some of the most challenging model instances. Notably, it precisely captures properties such as energy, the correlation function, and the overlap probability distribution.

STATE OF THE ART

Some common architectures used for P_{NN} are normalizing flows [20–23] and diffusion models [24]. In this paper, we will however focus on autoregressive models [10], which make use of the factorization:

$$\begin{aligned} P_{\text{GB}}(\boldsymbol{\sigma}) &= P(\sigma_1)P(\sigma_2 \mid \sigma_1)P(\sigma_3 \mid \sigma_1, \sigma_2) \times \\ &\times \cdots P(\sigma_n \mid \sigma_1, \dots, \sigma_{n-1}) = \prod_{i=1}^n P(\sigma_i \mid \boldsymbol{\sigma}_{<i}), \end{aligned} \quad (6)$$

where $\boldsymbol{\sigma}_{<i} = (\sigma_1, \sigma_2, \dots, \sigma_{i-1})$, so that states can then be generated using *ancestral sampling*, i.e. generating first σ_1 , then σ_2 conditioned on the sampled value of σ_1 , then σ_3 conditioned to σ_1 and σ_2 and so on. The factorization in (6) is exact, but computing $P(\sigma_i \mid \boldsymbol{\sigma}_{<i})$ exactly generally requires a number of operations scaling exponentially with N . Hence, in practice, P_{GB} is approximated by P_{NN} that takes the form in Eq. (6) where each individual term $P(\sigma_i \mid \boldsymbol{\sigma}_{<i})$ is approximated using a small set of parameters. Note that the unsupervised problem of approximating P_{GB} is now formally translated into a supervised problem of learning the output, i.e. the probability $\pi_i \equiv P(\sigma_i = +1 \mid \boldsymbol{\sigma}_{<i})$, as a function

of the input $\sigma_{<i}$. The specific way in which this approximation is carried out depends on the architecture. In this section we will describe some common autoregressive architectures found in literature, for approximating the function $\pi_i(\sigma_{<i})$.

- In the **Neural Autoregressive Distribution Estimator (NADE)** architecture [11], the input $\sigma_{<i}$ is encoded into a vector \mathbf{y}_i of size N_h using

$$\mathbf{y}_i = \Psi(\underline{A}\sigma_{<i} + \mathbf{B}), \quad (7)$$

where $\mathbf{y}_i \in \mathbb{R}^{N_h}$, $\underline{A} \in \mathbb{R}^{N_h \times N}$ and $\sigma_{<i}$ is the vector of the spins in which the spins $l \geq i$ have been masked, i.e. $\sigma_{<i} = (\sigma_1, \sigma_2, \dots, \sigma_{i-1}, 0, \dots, 0)$. $\mathbf{B} \in \mathbb{R}^{N_h}$ is the bias vector and Ψ is an element-wise activation function. Note that A and \mathbf{B} do not depend on the index i , i.e. they are shared across all spins. The information from the hidden layer is then passed to a fully connected layer

$$H_i = \Psi(\mathbf{V}_i \cdot \mathbf{y}_i + C_i) \quad (8)$$

where $\mathbf{V}_i \in \mathbb{R}^{N_h}$ and $C_i \in \mathbb{R}$. Finally, the output probability is obtained by applying a sigmoid function to the output, $\pi_i = S(H_i)$. The Nade Architecture uses $\mathcal{O}(N \times N_h)$ parameters. However, the choice of the hidden dimension N_h and how it should be related to N is not obvious. For this architecture to work well in practical applications, N_h needs to be $\mathcal{O}(N)$, thus leading to $\mathcal{O}(N^2)$ parameters [11].

- The **Masked Autoencoder for Distribution Estimator (MADE)** [26] is a generic dense architecture with the addition of the autoregressive requirement, obtained by setting, for all layers l in the network, the weights W_{ij}^l between node j at layer l and node i at layer $l+1$ equal to 0 when $i \geq j$. Between one layer and the next one adds nonlinear activation functions and the width of the hidden layers can also be increased. The MADE architecture, despite having high expressive power, has at least $\mathcal{O}(N^2)$ parameters, which makes it poorly scalable.
- **Autoregressive Convolutional Neural Network (CNN)** architectures, such as Pixel-CNN [27], are networks that implement a CNN structure but superimpose the autoregressive property. These architecture typically use translationally invariant kernels ill-suited to study disordered models and remain limited to two-dimensional systems.
- The **TwoBo (two-body interaction)** architecture [25] is derived from the observation that, given the Gibbs-Boltzmann probability in Eq. (1) and the Hamiltonian in Eq. (3), the probability π_i can be exactly rewritten as [28]

$$\pi_i(\sigma_{<i}) = S(2\beta h_i^i + 2\beta H_i + \rho_i(\mathbf{h}^i)), \quad (9)$$

where S is the sigmoid function, ρ_i is a highly non-trivial function and the $\mathbf{h}^i = \{h_i^i, h_{i+1}^i, \dots, h_N^i\}$ are defined as:

$$h_l^i = \sum_{f < i} J_{lf} \sigma_f \quad \text{for } l \geq i. \quad (10)$$

Therefore, the TwoBo architecture first computes the vector \mathbf{h}^i , then approximates $\rho_i(\mathbf{h}^i)$ using a Neural Network (for instance, a Multilayer Perceptron) and finally computes Eq. (9) using a skip connection (for the term $2\beta h_i^i$) and a sigmoid activation. By construction, in a two-dimensional model with $N = L^2$ variables and nearest-neighbor interactions, for given i only $\mathcal{O}(L = \sqrt{N})$ of the h_l^i are non-zero, see Ref. [25, Fig.1]. Therefore, the TwoBo architecture has $\mathcal{O}(N^{\frac{3}{2}})$ parameters in the two-dimensional case. However, the scaling becomes worse in higher dimensions d , i.e. $\mathcal{O}(N^{\frac{2d-1}{d}})$ and becomes the same as MADE (i.e. $\mathcal{O}(N^2)$) for random graphs. Additionally, the choice of the h_l^i , although justified mathematically, does not have a clear physical interpretation: the TwoBo architecture takes into account far away spins which, however, should matter much when N is large.

To summarize, the NADE, MADE and TwoBo architectures all need $\mathcal{O}(N^2)$ parameters for generic models defined on random graph structures. TwoBo has less parameters for models defined on d -dimensional lattices, but still $\mathcal{O}(N^{\frac{2d-1}{d}}) \gg \mathcal{O}(N)$. CNN architectures with translationally invariant kernels have less parameters, but are not suitable for disordered systems and remain limited to $d = 2$.

To solve these problems, we present here the new, physically motivated 4N architecture that has $\mathcal{O}(\mathcal{A}N)$ parameters, with a prefactor \mathcal{A} that remains finite for $N \rightarrow \infty$ and is interpreted as the correlation length of the system, as we show in the next section.

RESULTS

The 4N architecture

The 4N architecture (Fig. 1) computes the probability $\pi_i \equiv P(\sigma_i = +1 \mid \sigma_{<i})$ by propagating the h_l^i , defined as in TwoBo, Eq. (10), through a Graph Neural Network (GNN) architecture. The variable h_l^i is interpreted as the local field induced by the frozen variables $\sigma_{<i}$ on spin l . Note that in 4N, we consider all possible values of $l = 1, \dots, N$, not only $l \geq i$ as in TwoBo. The crucial difference with TwoBo is that only the fields in a finite neighborhood of variable i need to be considered, because the initial values of the fields are propagated through a series of GNN layers that take into account the locality of the physical problem. During propagation, fields are weighted using layer and edge dependent layers together

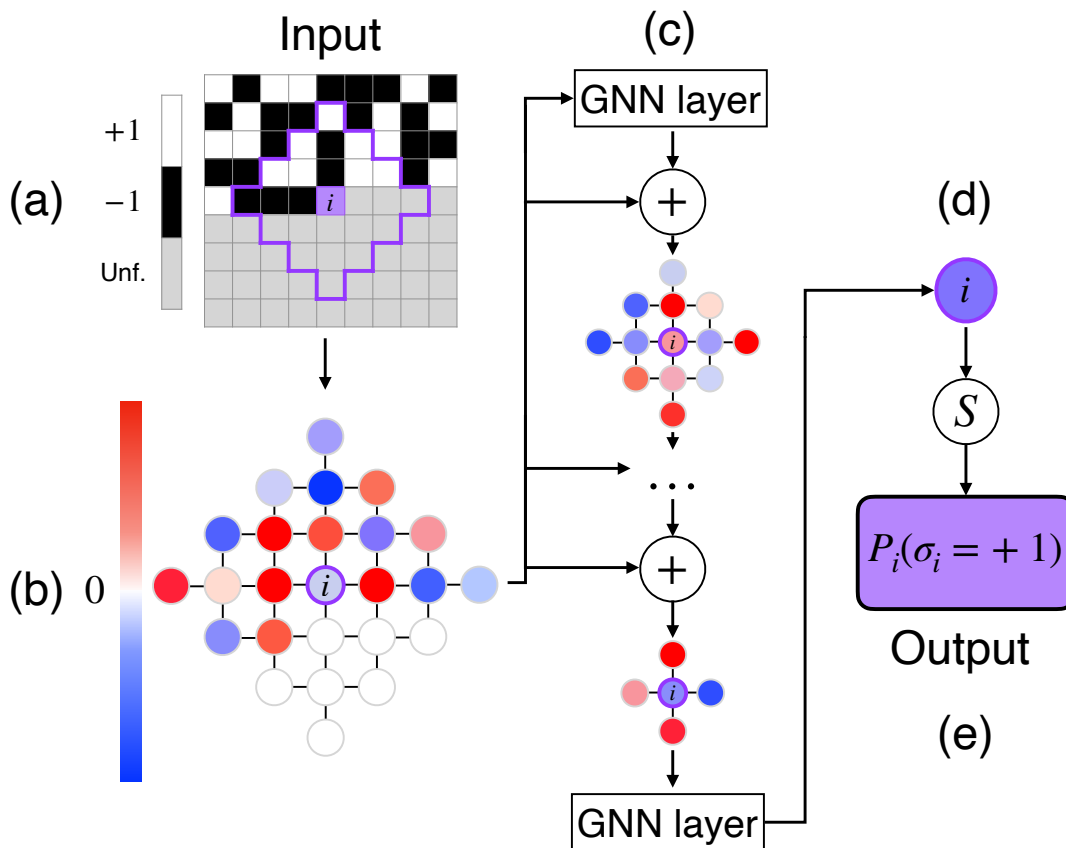


FIG. 1. Schematic representation of the 4N architecture implemented on a two-dimensional lattice model with nearest-neighbors interactions. (a) We want to estimate the probability $\pi_i \equiv P(\sigma_i = +1 \mid \sigma_{<i})$ that the spin i (in purple) has value $+1$ given the spins $< i$ (in black and white). The spins $> i$ (in grey) have not yet been fixed. (b) We compute the values of the local fields $h_i^{i,(0)}$ as in Eq. (10), for l in a neighborhood of i of size ℓ , indicated by a purple contour in (a). Notice that spins l that are not in the neighborhood of one of the fixed spin have $h_i^{i,(0)} = 0$ and are indicated in white in (b). (c) In the main cycle of the algorithm, we apply a series of ℓ GNN layers with the addition of skip connections. (d) The final GNN layer is not followed by a skip connection and yields the final values of the field $h_i^{i,(\ell)}$. (e) π_i is estimated by applying a sigmoid function to $h_i^{i,(\ell)}$. Periodic (or other) boundary conditions can be considered, but are not shown here for clarity.

with the couplings J_{ij} and the inverse temperature β . After each layer of the network (except the final one), a skip connection to the initial configuration is added. After the final layer, a sigmoidal activation is applied to find π_i . Details are given in the Methods section.

More precisely, because GNN updates are local, and there are ℓ of them, in order to compute the final field on i we only need to consider fields at distance at most ℓ . Therefore, the number of computations required to compute π_i is $\mathcal{O}(\ell^d)$, thus granting the generation of a new configuration in $\mathcal{O}(\ell^d \times N)$ steps. It is therefore crucial to assess how the number of layers ℓ should scale with the system size N .

The benchmark Gibbs-Boltzmann distribution

In this paper, in order to test the 4N architecture on a prototypically hard-to-sample problem, we will con-

sider the Edwards-Anderson spin glass model, described by the Hamiltonian in Eq. (3) for Ising spins, where we set $H_i = 0$ for simplicity. The couplings are chosen to be non-zero only for neighboring pairs $\langle i, j \rangle$ on a two-dimensional hypercubic lattice. Non-zero couplings J_{ij} are independent random variables, identically distributed according to either a normal or a Rademacher distribution. This model was also used as a benchmark in Refs. [11, 15].

While this model has no finite-temperature spin glass transition, sampling it via standard local MCMC becomes extremely hard for $\beta \gtrsim 1.5$ [15]. To this day, the best option for sampling this model at lower temperature is parallel tempering (PT), which we used to construct a sample of $M = 2^{16}$ equilibrium configurations for several instances of the model and at several temperatures. Details are given in the Methods section.

The PT-generated training set is used to train the 4N architecture, independently for each instance and each

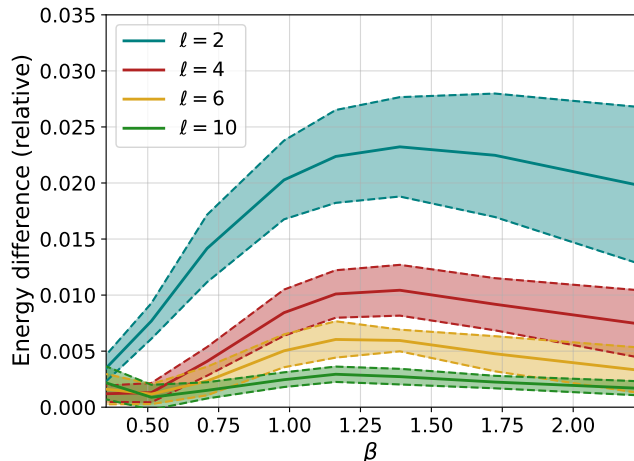


FIG. 2. Relative difference in mean energy between the configurations generated by the 4N architecture and by PT, for different numbers of layers ℓ and different values of the inverse temperature β . Solid lines indicate averages over 10 different instances, while the dashed lines and the colored area identify the region corresponding to plus or minus one standard deviation.

temperature. Remember that the goal here is to test the expressivity of the architecture, which is why we train it in the best possible situation, i.e. by maximizing the likelihood of equilibrium configurations at each temperature. Once the 4N model has been trained, we perform several comparisons that are reported in the following.

Energy

We begin by comparing the mean energy of the configurations generated by the model with the mean energy of the configurations generated via parallel tempering, which is important because the energy plays an important role in the Metropolis reweighing scheme of Eq. (5). Fig. 2 shows the relative energy difference, as a function of inverse temperature β and number of layers ℓ , averaged over 10 different instances of the disorder. First, it is clear that adding layers improves results remarkably. We stress that, since the activation functions of our network are linear, adding layers only helps in taking into account spins that are further away. Second, we notice that the relative error found when using 6 layers or more is small for all temperatures considered. Finally, we notice that the behaviour of the error is non-monotonic, and indeed appears to decrease for low temperatures even for networks with few layers.

Entropy and Kullback-Leibler divergence

Next, we consider the Kullback-Leibler divergence between the learned probability distribution P_{NN} and the

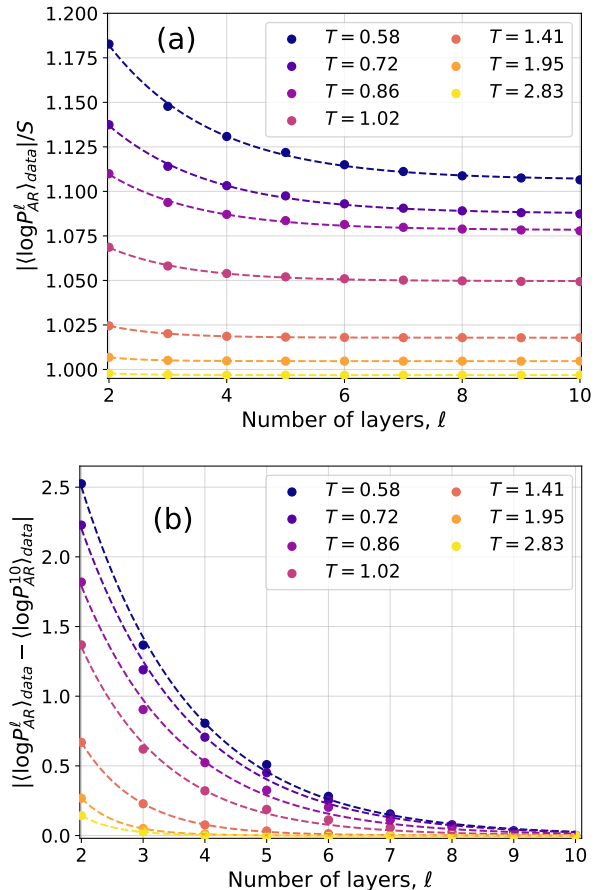


FIG. 3. (a) Ratio between the cross-entropy $|\langle \log P_{NN}^\ell \rangle_{\text{data}}|$ and the Gibbs-Boltzmann entropy S_{GB} for different values of the temperature T and of the number of layers ℓ . Both $|\langle \log P_{NN}^\ell \rangle_{\text{data}}|$ and S_{GB} are averaged over 10 samples. Dashed lines are exponential fits in the form $Ae^{-\ell/\bar{\ell}} + C$. (b) Absolute difference between $|\langle \log P_{NN}^\ell \rangle_{\text{data}}|$ at various ℓ and at $\ell = 10$. Dashed lines are exponential fits in the form $Ae^{-\ell/\bar{\ell}}$.

target probability distribution, $D_{KL}(P_{GB} \parallel P_{NN})$. Indicating with $\langle \cdot \rangle_{GB}$ the average with respect to P_{GB} , we have

$$D_{KL}(P_{GB} \parallel P_{NN}) = \langle \log P_{GB} \rangle_{GB} - \langle \log P_{NN} \rangle_{GB}. \quad (11)$$

The first term $\langle \log P_{GB} \rangle_{GB} = -S_{GB}(T)$ is minus the entropy of the Gibbs-Boltzmann distribution and does not depend on P_{NN} , hence we focus on the cross-entropy $-\langle \log P_{NN} \rangle_{GB}$ as a function of the number of layers for different temperatures. Minimizing this quantity corresponds to minimizing the KL divergence. In the case of perfect learning, i.e. $D_{KL} = 0$, we have $-\langle \log P_{NN} \rangle_{GB} = S_{GB}(T)$. In Fig. 3 we compare the cross-entropy, estimated as $-\langle \log P_{NN} \rangle_{\text{data}}$ on the data generated by PT, with $S_{GB}(T)$ computed using thermodynamic integration. We find a good match for large enough ℓ , indicating an accurate training of the 4N model that does not suffer from mode collapse.

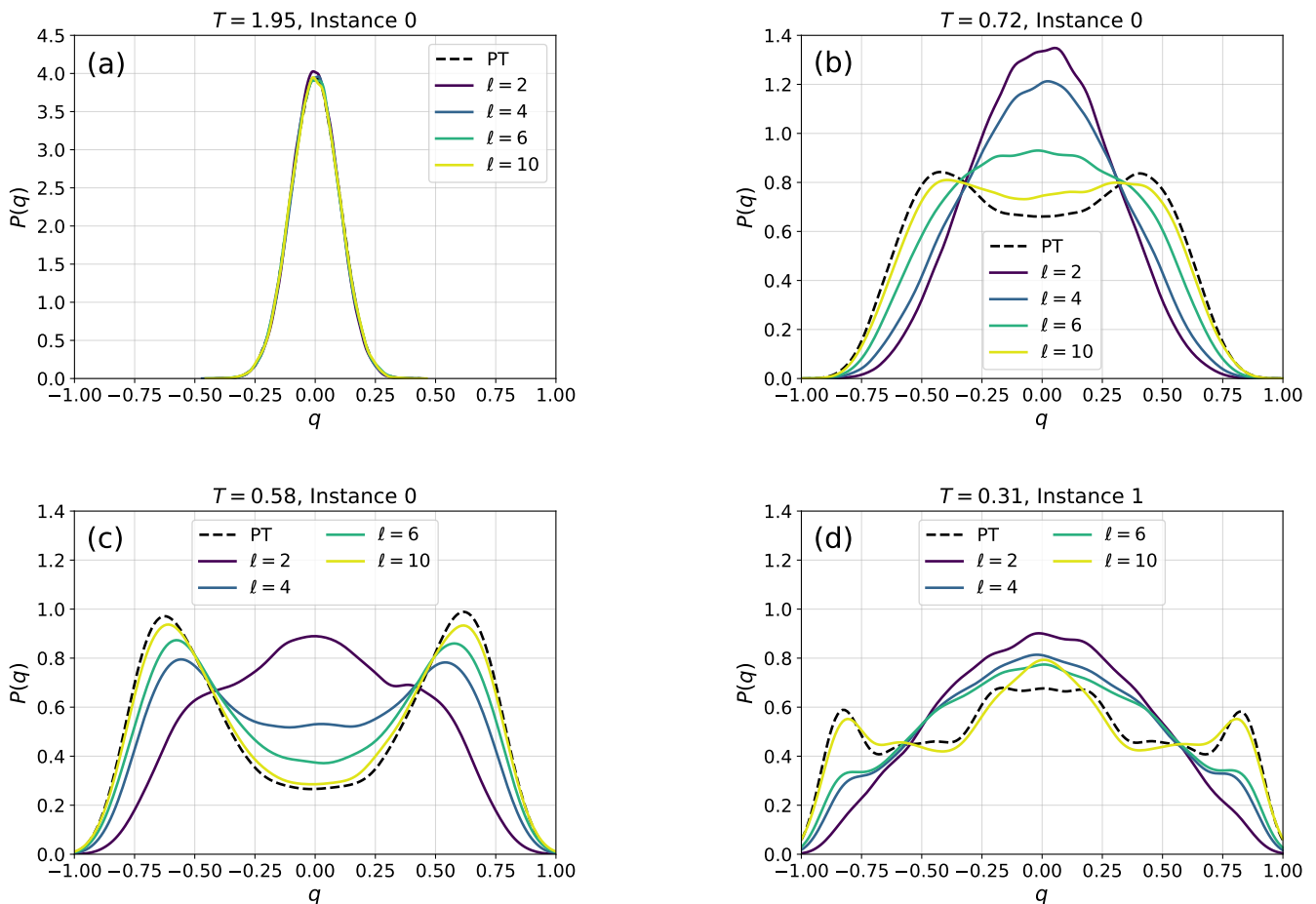


FIG. 4. Examples of the probability distribution of the overlap, $P(q)$, for different instances of the disorder and different temperatures. Solid color lines correspond to configurations generated using $4N$, while dashed black lines correspond to the $P(q)$ obtained from equilibrium configurations generated via PT. (a) At high temperature, even a couple of layers are enough to reproduce well the distribution. (b) At lower temperatures more layers are required, as expected because of the increase of the correlation length and of the complexity of the Gibbs-Boltzmann distribution. (c) Even lower temperature for the same instance. (d) A test on a particularly complex instance shows that $4N$ is capable to learn even non-trivial forms of $P(q)$.

In order to study more carefully how changing the number of layers affects the accuracy of the training, in Fig. 3 we have also shown the difference $|\langle \log P_{AR}^\ell \rangle_{data} - \langle \log P_{AR}^{10} \rangle_{data}|$ as a function of the number of layers ℓ for different temperatures. The plots are compatible with an exponential decay in the form $Ae^{-\ell/\bar{\ell}}$, with $\bar{\ell}$ thus being an estimate of the number of layers above which the $4N$ architecture becomes accurate. We thus need to understand how $\bar{\ell}$ changes with temperature and system size. To do so, we need to introduce appropriate correlation functions, as we do next.

Overlap distribution function

In order to show that the $4N$ architecture is able to capture more complex features of the Gibbs-Boltzmann distribution, we have considered a more sensitive ob-

servable: the probability distribution of the overlap, $P(q)$. The overlap q between two configurations of spins $\boldsymbol{\sigma}^1 = \{\sigma_1^1, \sigma_2^1, \dots, \sigma_N^1\}$ and $\boldsymbol{\sigma}^2 = \{\sigma_1^2, \sigma_2^2, \dots, \sigma_N^2\}$ is a central quantity in spin glass physics, and is defined as:

$$q_{12} = \frac{1}{N} \boldsymbol{\sigma}^1 \cdot \boldsymbol{\sigma}^2 = \frac{1}{N} \sum_{i=1}^N \sigma_i^1 \sigma_i^2. \quad (12)$$

The histogram of $P(q)$ is obtained by considering many pairs of configurations, independently taken from either the PT-generated training set, or by generating them with the $4N$ architecture. Examples for two different instances at several temperatures are shown in Fig. 4. At high temperatures, even very few layers are able to reproduce the distribution of the overlaps. When going to lower temperatures, and to more complex shapes of $P(q)$, however, the number of layers that is required to have a good approximation of $P(q)$ increases. This result is compatible with the intuitive idea that an increasing

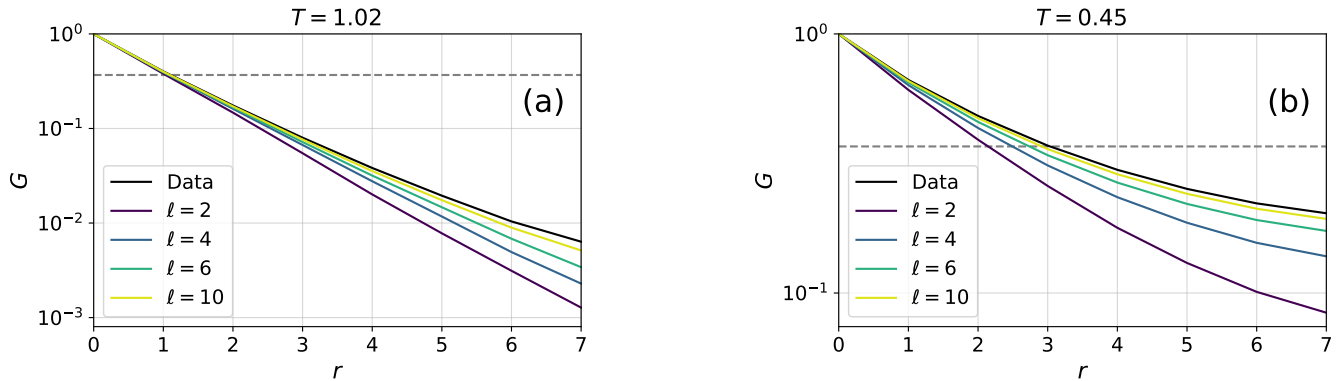


FIG. 5. Comparison between the spatial correlation functions obtained from 4N and those obtained from PT, at different high (a) and low (b) temperatures and for different number of layers. The grey dashed lines correspond to the value $1/e$ that defines the correlation length ξ . Data are averaged over 10 instances.

number of layers is required to reproduce a system at low temperatures, where the correlation length is large.

As shown in the SI, the performance of 4N is on par with that of other algorithms with more parameters. Moreover, with a suitable increase of the number of layers, 4N is also able to achieve satisfactory results when system's size increases.

Spatial correlation function

To better quantify spatial correlations, from the overlap field, a proper correlation function for a spin glass system can be defined as [29]

$$G(r) = \frac{1}{L^2 \Omega(r)} \sum_{i,j:d_{ij}=r} \overline{\langle q_i q_j \rangle}, \quad (13)$$

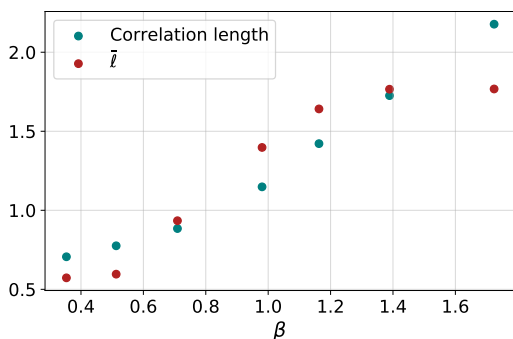


FIG. 6. Comparison between the correlation length ξ and the decay parameter $\bar{\ell}$ of the exponential fit as a function of the inverse temperature β . Both data sets are averaged over 10 instances. The data are limited to $T \geq 0.58$ because below that temperature the finite size of the sample prevents us to obtain a reliable proper estimate of the correlation length.

where $r = d_{ij}$ is the lattice distance of sites i, j , $q_i = \sigma_i^1 \sigma_i^2$ is the local overlap, and $\Omega(r) = \sum_{i:d_{ij}=r} 1$ is the volume of a ball of radius r around any given site. Note that in this way $G(0) = 1$ by construction. Results for $G(r)$ at various temperatures are shown in Fig. 5. It is clear that increasing the number of layers leads to a better agreement at lower temperatures. Interestingly, architectures with a lower numbers of layers produce a smaller correlation function at any distance, which shows that upon increasing the number of layers the 4N architecture is effectively learning the correlation of the Gibbs-Boltzmann measure.

To quantify this intuition, we extract from the exact $G(r)$ of the EA model a correlation length ξ , from the relation $G(\xi) = 1/e$. Then, we compare ξ with $\bar{\ell}$, i.e. the number of layers above which the model becomes accurate, extracted from Fig. 3. These two quantities are compared in Fig. 6 as a function of temperature, showing that they are roughly proportional. We are thus able to introduce a physical criterion to fix the optimal number of layers needed for the 4N architecture to perform well: ℓ must be a multiple of the correlation length ξ of the model at that temperature. We conclude that, for a model with a correlation length ξ that remains finite for $N \rightarrow \infty$, the 4N architecture requires $(c + 1) \times \ell \times N$ parameters and $\mathcal{O}(\ell^d \times N)$ operations to generate a new configuration, with ℓ proportional to ξ , hence achieving the desired $\mathcal{O}(N)$ scaling with system size both for the number of parameters and the number of operations.

DISCUSSION

In this work we have introduced a new, physics-inspired 4N architecture for the approximation of the Gibbs-Boltzmann probability distribution of a spin glass system of N spins. The 4N architecture is inspired by the previously introduced TwoBo [25], but it implements explicitly the locality of the physical model via a Graph

Neural Network structure.

The 4N network possesses many desirable properties. (i) The architecture has a physical interpretation, with the required number of layers being directly linked to the correlation length of the original data. (ii) As a consequence, if the correlation length of the model is finite, the required number of parameters for a good fit scales linearly in the number of spins, thus greatly improving the scalability with respect to previous architectures. (iii) The architecture is very general, and can be applied to lattices in all dimensions as well as arbitrary interaction graphs without losing the good scaling of the number of parameters, as long as the average connectivity remains finite. It can also be generalized to systems with more than two-body interactions by using a factor graph representation in the GNN layers.

As a benchmark study, we have tested that the 4N architecture is powerful enough to reproduce key properties of the two-dimensional Edwards-Anderson spin glass model, such as the energy, the correlation function and the probability distribution of the overlap.

Having tested that 4N achieves the best possible scaling with system size while being expressive enough, the next step is to check whether it is possible to apply an iterative, self-consistent procedure to automatically train the network at lower and lower temperatures without the aid of training data generated with a different algorithm (here, parallel tempering). This would allow to set up a simulated tempering procedure with a good scaling in the number of variables, with applications not only in the simulation of disordered systems but in the solution of optimization problems as well. Whether setting up such a procedure is actually possible will be the focus of future work.

METHODS

Details of the 4N architecture

The Nearest Neighbors Neural Network (4N) architecture uses a GNN structure to respect the locality of the problem, as illustrated in Fig. 1. The input, given by the local fields computed from the already fixed spins, is passed through ℓ layers of weights W_{ij}^k . Each weight corresponds to a directed nearest neighbor link $i \leftarrow j$ (including $i = j$) and $k = 1, \dots, \ell$, therefore the network has a total number of parameters equal to $(c+1) \times \ell \times N$, i.e. linear in N as long as the number of layers and the model connectivity remain finite.

The operations performed in order to compute $\pi_i = P(\sigma_i = 1 \mid \sigma_{<i})$ are the following:

1. **initialize** the local fields from the input spins $\sigma_{<i}$:

$$h_l^{i,(0)} = \sum_{f(<i)} J_{lf} \sigma_f, \quad \forall l : |i - l| \leq \ell.$$

2. **iterate** the GNN layers $\forall k = 1, \dots, \ell - 1$:

$$h_l^{i,(k)} = \phi^k \left[\beta W_{ll}^k h_l^{i,(k-1)} + \sum_{j \in \partial l} \beta J_{lj} W_{lj}^k h_j^{i,(k-1)} \right] + h_l^{i,(0)},$$

where the sum over $j \in \partial l$ runs over the neighbors of site l . The fields are computed $\forall l : |i - l| \leq \ell - k$, see Fig. 1.

3. **compute** the field on site i at the final layer,

$$h_i^{i,(\ell)} = \phi^\ell \left[\beta W_{ii}^\ell h_i^{i,(\ell-1)} + \sum_{j \in \partial i} \beta J_{ij} W_{ij}^\ell h_j^{i,(\ell-1)} \right].$$

4. **output** $\pi_i = P(\sigma_i = 1 \mid \sigma_{<i}) = S[2h_i^{i,(\ell)}]$.

Here $S(x) = 1/(1 + e^{-x})$ is the sigmoid function and $\phi^k(x)$ are layer-specific functions that can be used to introduce non-linearities in the system. The fields $h_l^{i,(0)} = \xi_{il}$ in the notation of the TwoBo architecture. Differently from TwoBo, however, 4N uses all the $h_l^{i,(0)}$, instead of the ones corresponding to spins that have not yet been fixed.

In practice, we have observed that the network with identity functions, i.e. $\phi^k(x) = x$ for all k , is sufficiently expressive, and using non-linearities does not seem to improve the results. Moreover, linear functions have the advantage of being easily explainable and faster, therefore we have chosen to use them in this work.

Spin update order

Autoregressive models such as 4N are based on an ordering of spins to implement Eq. (6). One can choose a simple raster scan (i.e., from left to right on one row and updating each row from top to bottom sequentially) or any other scheme of choice. In this work, we have adopted a spiral scheme, in which the spins at the edges of the system are updated first, and then one moves in spirals towards the central spins. As shown in the SI, it appears as 4N performs better, for equal training conditions, when the spins are updated following a spiral scheme with respect to, for instance, a raster scheme.

Building the training data

We use as training set of $M = 2^{16}$ configurations obtained at several temperatures using a Parallel Tempering algorithm for different instances of the couplings J_{ij} , and for a 16x16 two-dimensional square lattice with periodic boundary conditions. Data were gathered in runs of 2^{27} steps by considering 2^{26} steps for thermalization and then taking one configuration each 2^{10} steps. Temperature swap moves, in which one swaps two configurations at nearby temperature, were attempted once every

32 normal Metropolis sweeps. The choice of $M = 2^{16}$ was motivated based on previous studies of the same model [15].

Model training

The training has been carried out maximizing the likelihood of the data, a procedure which is equivalent to minimizing the KL divergence $D_{\text{KL}}(P_{\text{GB}} \parallel P_{\text{NN}})$, with P_{GB} estimated by the training set. We used an ADAM optimizer with batch size 100 for 80 epochs, early stopping with patience 10, learning rate 0.01 with exponential decay in time.

ACKNOWLEDGMENTS

We especially thank Indaco Biazzo and Giuseppe Carleo for several important discussions on their TwoBo architecture that motivated and inspired the present study. We also thank Giulio Biroli, Patrick Charbonneau, Simone Ciarella, Marylou Gabrié, Leonardo Galliano, Jeanne Trinquier, Martin Weigt and Lenka Zdeborová for useful discussions. The research has received financial support from ICSC - Italian Research Center on High-Performance Computing, Big Data, and Quantum Computing, funded by the European Union - NextGenerationEU.

-
- [1] Ulli Wolff. Collective monte carlo updating for spin systems. 62(4):361–364. Publisher: American Physical Society.
 - [2] Andrea Ninarello, Ludovic Berthier, and Daniele Coslovich. Models and algorithms for the next generation of glass transition studies. *Phys. Rev. X*, 7:021039, Jun 2017.
 - [3] E. Marinari and G. Parisi. Simulated tempering: A new monte carlo scheme. *Europhysics Letters*, 19(6):451, jul 1992.
 - [4] J. Houdayer. A cluster monte carlo algorithm for 2-dimensional spin glasses. 22(4):479–484.
 - [5] Giuseppe Carleo and Matthias Troyer. Solving the quantum many-body problem with artificial neural networks. 355(6325):602–606. Publisher: American Association for the Advancement of Science.
 - [6] Samuel Tamagnone, Alessandro Laio, and Marylou Gabrié. Coarse grained molecular dynamics with normalizing flows. *arXiv preprint arXiv:2406.01524*, 2024.
 - [7] Gerhard Jung, Rinske M Alkemade, Victor Bapst, Daniele Coslovich, Laura Filion, François P Landes, Andrea Liu, Francesco Saverio Pezzicoli, Hayato Shiba, Giovanni Volpe, et al. Roadmap on machine learning glassy liquids. *arXiv preprint arXiv:2311.14752*, 2023.
 - [8] Leonardo Galliano, Riccardo Rende, and Daniele Coslovich. Policy-guided monte carlo on general state spaces: Application to glass-forming mixtures. *arXiv preprint arXiv:2407.03275*, 2024.
 - [9] Simone Ciarella, Dmytro Khomenko, Ludovic Berthier, Felix C Mocanu, David R Reichman, Camille Scalliet, and Francesco Zamponi. Finding defects in glasses through machine learning. *Nature Communications*, 14(1):4229, 2023.
 - [10] Dian Wu, Lei Wang, and Pan Zhang. Solving statistical mechanics using variational autoregressive networks. 122(8):080602. Publisher: American Physical Society.
 - [11] B. McNaughton, M. V. Milošević, A. Perali, and S. Pilati. Boosting monte carlo simulations of spin glasses using autoregressive neural networks. 101(5):053312. Publisher: American Physical Society.
 - [12] Martin J. A. Schuetz, J. Kyle Brubaker, and Helmut G. Katzgraber. Combinatorial optimization with physics-inspired graph neural networks. 4(4):367–377. Publisher: Nature Publishing Group.
 - [13] Martin J. A. Schuetz, J. Kyle Brubaker, Zhihui Zhu, and Helmut G. Katzgraber. Graph coloring with physics-inspired graph neural networks. 4(4):043131. Publisher: American Physical Society.
 - [14] Changjun Fan, Mutian Shen, Zohar Nussinov, Zhong Liu, Yizhou Sun, and Yang-Yu Liu. Searching for spin glass ground states through deep reinforcement learning. 14(1):725. Publisher: Nature Publishing Group.
 - [15] Simone Ciarella, Jeanne Trinquier, Martin Weigt, and Francesco Zamponi. Machine-learning-assisted monte carlo fails at sampling computationally hard problems. *Machine Learning: Science and Technology*, 4(1):010501, 2023.
 - [16] Maria Chiara Angelini and Federico Ricci-Tersenghi. Modern graph neural networks do worse than classical greedy algorithms in solving combinatorial optimization problems like maximum independent set. 5(1):29–31.
 - [17] Stefan Boettcher. Inability of a graph neural network heuristic to outperform greedy algorithms in solving combinatorial optimization problems. *Nature Machine Intelligence*, 5(1):24–25, 2023.
 - [18] Changjun Fan, Mutian Shen, Zohar Nussinov, Zhong Liu, Yizhou Sun, and Yang-Yu Liu. Reply to: Deep reinforced learning heuristic tested on spin-glass ground states: The larger picture. *Nature communications*, 14(1):5659, 2023.
 - [19] Davide Ghio, Yatin Dandi, Florent Krzakala, and Lenka Zdeborová. Sampling with flows, diffusion and autoregressive neural networks: A spin-glass perspective. *arXiv preprint arXiv:2308.14085*, 2023.
 - [20] Jonas Köhler, Leon Klein, and Frank Noé. Equivariant flows: Exact likelihood generative learning for symmetric densities.
 - [21] Marylou Gabrié, Grant M. Rotskoff, and Eric Vandeneijnden. Adaptive monte carlo augmented with normalizing flows. 119(10):e2109420119. Publisher: Proceedings of the National Academy of Sciences.
 - [22] Manuel Dibak, Leon Klein, Andreas Krämer, and Frank Noé. Temperature steerable flows and boltzmann generators. 4(4):L042005. Publisher: American Physical Society.
 - [23] Michele Invernizzi, Andreas Krämer, Cecilia Clementi, and Frank Noé. Skipping the replica exchange ladder with normalizing flows. *The Journal of Physical Chemistry Letters*, 13(50):11643–11649, 2022.

- [24] Wenlin Chen, Mingtian Zhang, Brooks Paige, José Miguel Hernández-Lobato, and David Barber. Diffusive gibbs sampling. *arXiv preprint arXiv:2402.03008*, 2024.
- [25] Indaco Biazzo, Dian Wu, and Giuseppe Carleo. Sparse autoregressive neural networks for classical spin systems.
- [26] Mathieu Germain, Karol Gregor, Iain Murray, and Hugo Larochelle. Made: Masked autoencoder for distribution estimation. In *International conference on machine learning*, pages 881–889. PMLR, 2015.
- [27] Aaron Van den Oord, Nal Kalchbrenner, Lasse Espeholt, Oriol Vinyals, Alex Graves, et al. Conditional image generation with pixelcnn decoders. *Advances in neural information processing systems*, 29, 2016.
- [28] Indaco Biazzo. The autoregressive neural network architecture of the boltzmann distribution of pairwise interacting spins systems. *Communications Physics*, 6(1):296, 2023.
- [29] LA Fernandez, E Marinari, V Martin-Mayor, Giorgio Parisi, and JJ Ruiz-Lorenzo. Universal critical behavior of the two-dimensional ising spin glass. *Physical Review B*, 94(2):024402, 2016.

S1: Probability distribution of the overlap for $L = 32$

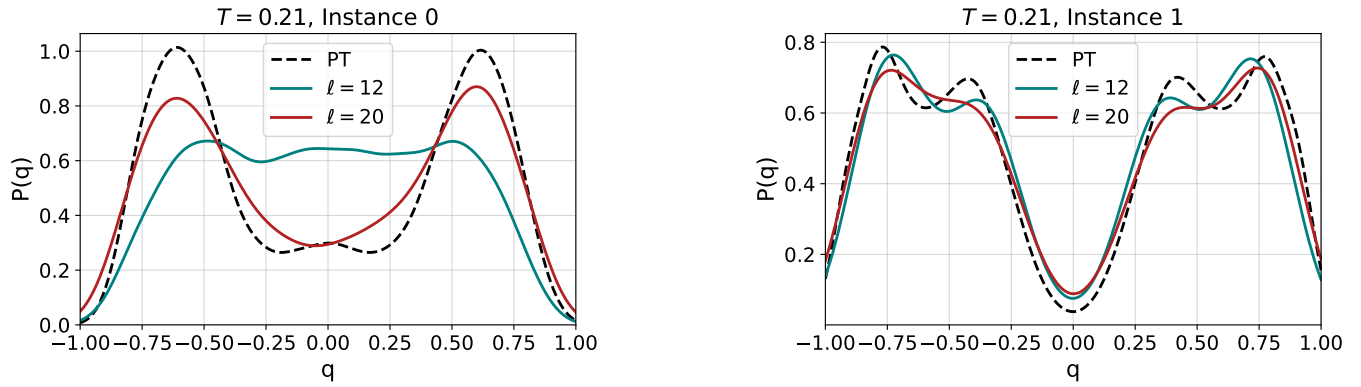


FIG. S1. Additional examples of the probability distribution of the overlap, $P(q)$, for different instances of the disorder and different temperatures for the $L = 32$, $N = 1024$ case. Solid color lines correspond to configurations generated using $4N$, while dashed black lines correspond to the $P(q)$ obtained via PT. With the increase of the system size, more layers are required in order to reproduce correctly the probability distribution of the overlap at lower temperatures, as expected by the fact that finite-size effects are less present.

S2: Comparison between different architectures

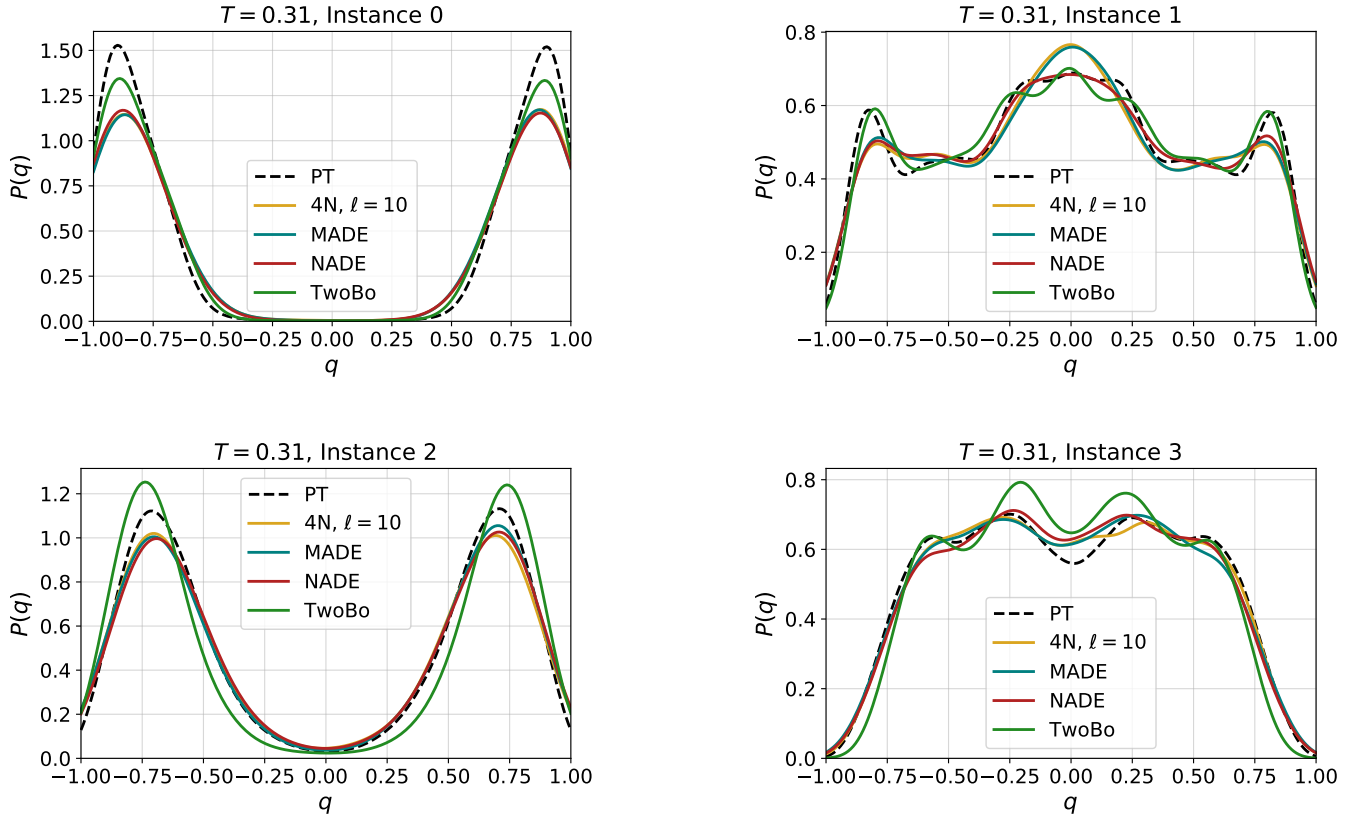


FIG. S2. Comparison of the probability distribution of the overlap obtained using different architectures: 4N with $\ell = 10$ layers (12580 parameters), shallow MADE (32640 parameters), NADE with $N_h = 64$ (32768 parameters) and TwoBo (7709 parameters). The black dashed line is obtained using data gathered via Parallel Tempering (PT), while solid color lines are obtained using the different architectures. 4N performs comparably or better than MADE and NADE despite having less parameters. Moreover, it also performs comparably to TwoBo. Despite the latter having fewer parameters in this $N = 256$ case, 4N has a better scaling when increasing the system size, $\mathcal{O}(N)$ compared to $\mathcal{O}(N^{\frac{3}{2}})$, as pointed out in the main text.

S3: Comparison between different update sequences

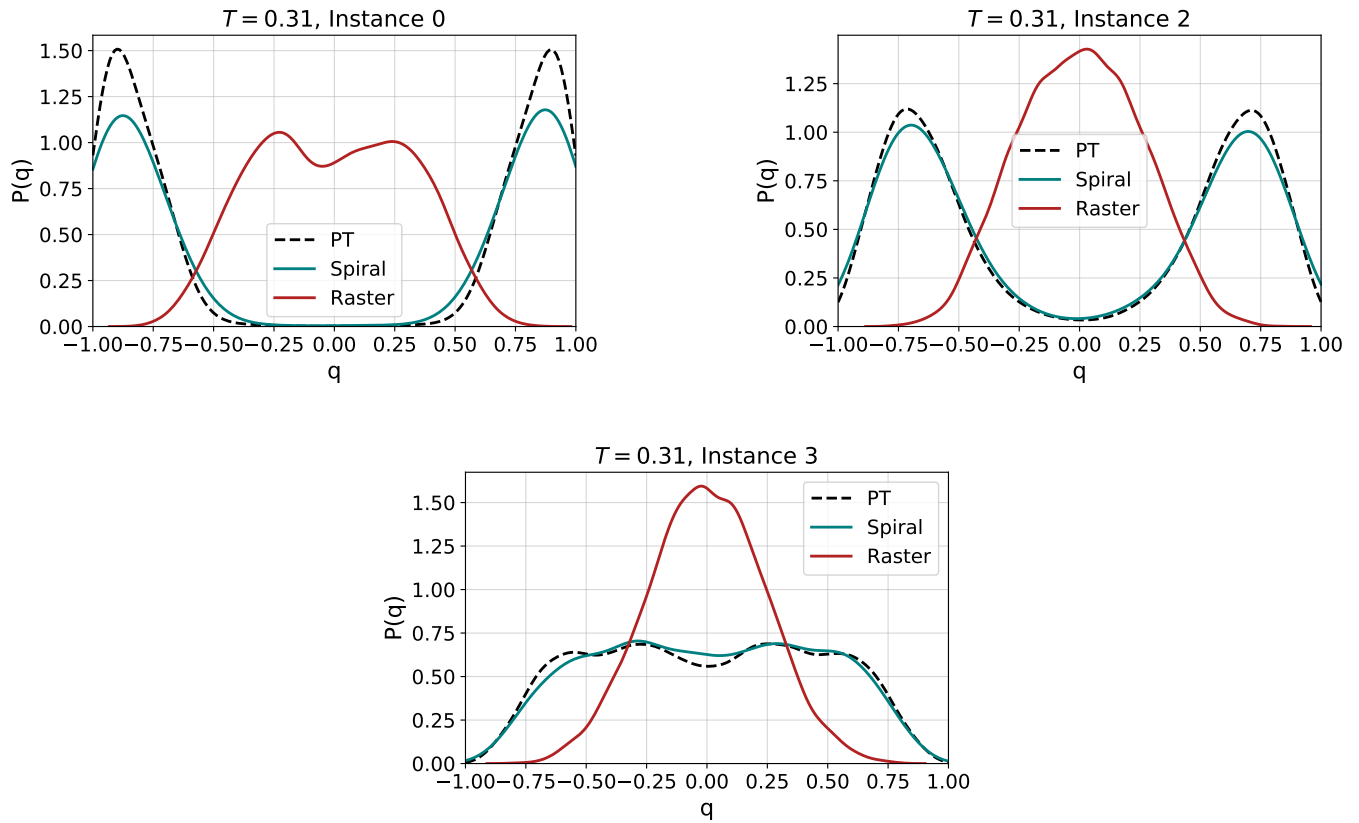


FIG. S3. Comparison of the probability distribution of the overlap obtained using different update sequences of the spins. The black dashed line is obtained using data gathered via Parallel Tempering (PT), while solid color lines are obtained using 4N with different sequence updates. *Spiral*: spins are update in a following a spiral going from the outside to the inside of the lattice; *Raster*: spins are updated row by row from left to right. It appears as the spiral update performs much better than the raster update for the 4N architecture in equal training conditions, something that is not observed when training, for instance, the MADE architecture. This effect could be related to the locality characteristics of the 4N architecture.